International Journal of Fluid Power, 2014
Vol. 15, No. 3, 121–137, http://dx.doi.org/10.1080/14399776.2014.977699

Taylor & Francis
Taylor & Francis Group

A novel design concept for variable delivery flow external gear pumps and motors

Ram Sudarsan Devendran* and Andrea Vacca

Maha Fluid Power Research Center, School of Mechanical Engineering, Purdue University 1500 Kepner Dr, Lafayette, IN 47905, USA

(*Received 1 August 2014; final version received 14 October 2014*)

This paper presents an original concept for variable delivery external spur gear machines, which combines the well-known advantages of these units (such as low cost, good reliability, acceptable efficiency) – traditionally fixed displacement – in a solution capable of varying the amount of flow displaced at each shaft revolution. The proposed design concept realizes a variable timing for the connections of each tooth space volume with the inlet and outlet ports, through a movable element ("slider") placed at the gears lateral side. The position of the slider determines the amount of flow displaced by the unit per revolution. In order to extend the range of flow variation achievable by the unit, an asymmetric involute tooth profile for the gears was proposed. A multi-objective genetic algorithm was used to optimize the design of the gears along with the design of the timing grooves in the slider. This algorithm is based on the HYGESIM (HYdraulic GEar machines Simulator) tool developed by the authors' research group for the evaluation of the performance of every particular design. The optimal design solution, capable of achieving 40% flow variation (from 100% to 60%), was realized in a working proof of concept and tested for the case of a pump, although the solution is in principle valid for both pumps and motors. Experimental results were in line with the numerical predictions and show the potential of this design concept of achieving flow variations in an energy efficient fashion, with volumetric and hydro-mechanical efficiency at reduced displacements in line with other state of the art variable displacement units.

Therefore, the proposed design can impact current applications for external gear pumps and motors, offering the additional flow-on-demand capability. Furthermore, it can be utilized in several other engineering applications in which traditional external gear machines were not a viable alternative because of their intrinsic fixed displacement nature.

Keywords: external gear pumps and motors; variable displacement; variable delivery; pump optimization; energy efficiency

1. Introduction

The well-known advantages of external gear machines (EGMs) such as low cost, compactness, reasonable operating efficiency and good reliability make them as one of the prominently used components in fluid power. EGMs are used as primary flow supply unit in many applications such as fuel injection systems, small mobile applications such as micro-excavators, turf and gardening machines. EGMs are also used in fixed applications such as hydraulic presses and forming machines. EGMs find also applications in auxiliary systems such as hydraulic power steering, fan-drive systems and as charge pump in hydrostatic transmissions.

In an EGM, as the shaft rotates, the fluid is transferred from the inlet to the outlet port through the peripheral of the gears, and the displacement of the fluid is achieved by the meshing of the teeth. At gears lateral side, grooves are used to realize proper connections of the inter-teeth volumes trapped between points of contact with the inlet/outlet ports, thus avoiding these volumes to be isolated during the meshing process. Therefore, grooves permit to utilize the full volumetric capacity of the unit, avoiding localized pressure peaks and fluid cavitation. In a pressure compensated EGM, such as the one represented in Figure 1, these grooves are realized in the sliding bushings (Figure 1(B)) – popularly known by the names of bearing blocks and pressure/thrust plates – used to realize optimal sealing of the tooth space volumes through a proper lubricating fluid film even at high operating pressures. In non-compensated EGM, these grooves are machined in the pump housing.

The above described principle of operation of an EGM makes these units inherently fixed displacement. This inability of adapting the fluid displaced per every revolution on the basis of user's requests makes EGMs unsuitable for applications in energy efficient system layout configurations which characterize many fluid power applications (Ivantysynova 1998, Murrenhoff *et al.* 2014). In these system configurations, variable displacement units can offer energy saving even greater than 50% compared to solutions based on fixed displacement units. Notwithstanding, fixed displacement units, such as EGMs, guarantee significant lower cost than same-size variable displacement units with superior reliability, and hence purporting the success of EGMs.

*Corresponding author. Email: rdevendr@purdue.edu

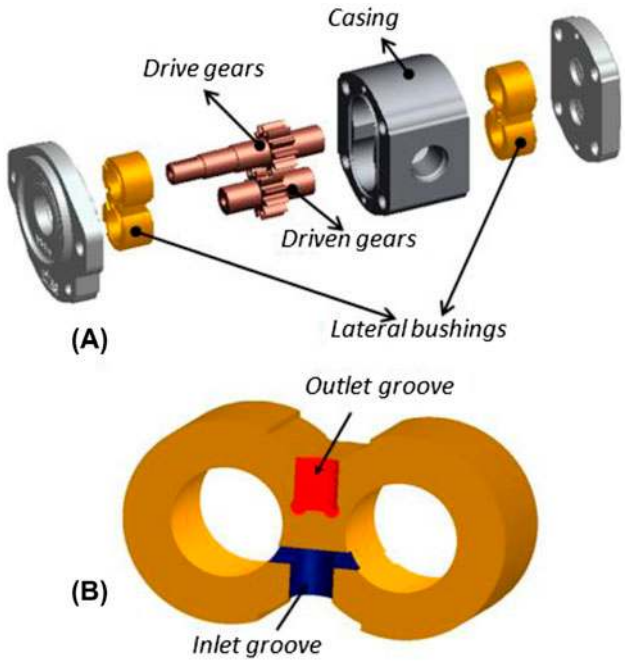

Figure 1. (A) Parts of an EGM (B) Grooves on the lateral bushing.

These factors have driven significant research towards the definition of a working concept for variable displacement EGMs. Past effort can be broadly categorized into two different sets of solutions: the first set of solutions consists in changing the meshing length of the gears. Several patents describe different solutions for this idea, by moving the gears axially (Bussi 1992, Winmill 2001, Clarke 2002, Hoji *et al*. 2008). The second set of solutions consists in changing the inter-axis distance between the gears, thereby affecting the meshing area of the gears (Reiners and Wiggermann 1960, Yang and Zhong 1987). However, all these solutions have not encountered successful commercialization. In fact, several major issues have to be faced to implement a viable and cost-effective solution to move the gears, which are the most loaded parts of the machine, guaranteeing at the same time good sealing and smooth transmission of power between the rotors.

Efforts to obtain inexpensive variable flow supply unit were also made at system level; in particular, solutions that combine fixed displacement pumps with fast switching valves controlled in PWM to obtain a variable output flow were proposed by several researchers (Tomlinson and Burrows 1992, Mahrenholz and Lumkes 2009, Rannow *et al.* 2009). Despite the theoretical validity of these so called "virtually variable displacement" solutions, their application in real systems is hampered by the 2limited time response of current on/off valves as well as compatibility issues of current fixed displacement pumps with the introduction of severe pressure pulsations.

Another solution described in the literature integrates an adjustable spool inside the pump used to manipulate the communication of the fluid in the displacement chamber to provide pressurized fluid from the outlet to the inlet thereby varying the discharge flow (Bowden 1989, 1990). Being based on conventional gear profiles, this idea – which presents some elements of similarity with the solution proposed in this paper – have not encountered success because the range of variability of the delivery flow could not exceed few point percent.

In the present study, a solution that implements a variable timing of the connections of the displacement chambers (the tooth space volumes, TSVs) with the inlet/output port is proposed (§2). This solution, described in details in the next section, preserves the compactness, reliability and low cost features typical of an EGM and permits to achieve a partial control of the flow displaced by the unit, in a range that depends on the profile of the gears. The novel design concept is based on the use of asymmetric involute and trochoid profiles for the gears, which are used to maximize the range of flow variation achievable by the unit (§3 and §4). As described in §5 and §6, an optimization process was performed to find the optimal profile of the gears, permitting to achieve a displacement variation range between 68% and 100% of maximum displacement. The numerical optimization process is based on a genetic algorithm which utilizes the simulation tool HYGESim (HYdraulic GEar machines Simulator) which is being developed by the authors' research group for over several years. In this study, the HYGESim tool was extended to be capable of simulating gear machines with asymmetric teeth profiles. The proposed design is also conceived to maximize the performance levels, in terms of delivery flow pulsations – responsible of noise emissions and vibrations – volumetric efficiency, internal pressure peaks and cavitation onset which occur in during the meshing process. Simulation results for the chosen design are presented in §7.

The displacement variation range was limited by some requirements of the experimental prototype chosen for the validation tests (§8). A wider displacement variation range, in the order of 50% – 100% could be achievable by removing these constraints.

2. Proposed design concept

The proposed concept is based on the realization of a variable timing for the connections of the TSVs with the inlet/outlet grooves. The variation in the timing of the connections is achieved by the introduction of a movable element – hereafter called "slider" – in the standard EGM design. Figure 2 depicts the introduction of the slider in the sliding lateral bushing block of a pressure compensated EGM, which is also the reference design case in this study. The position of the slider determines the amount of flow displaced by the unit per revolution, for both the cases of pumps and motors.

In order to understand the working principle of the proposed variable delivery (VD) EGM, the detailed displacing action of an EGM is described in Figure 3,

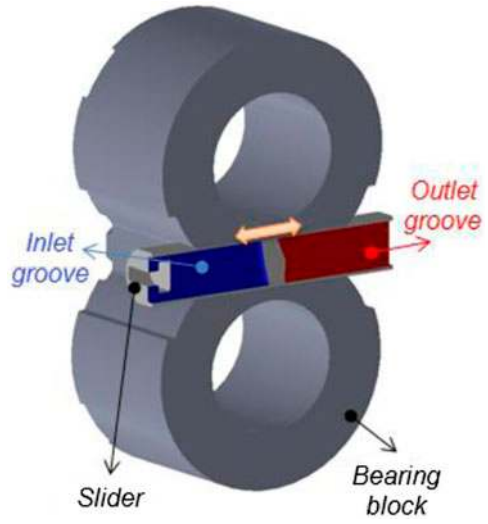

Figure 2. Slider placed inside the bearing block for achieving variable flow in an EGM.

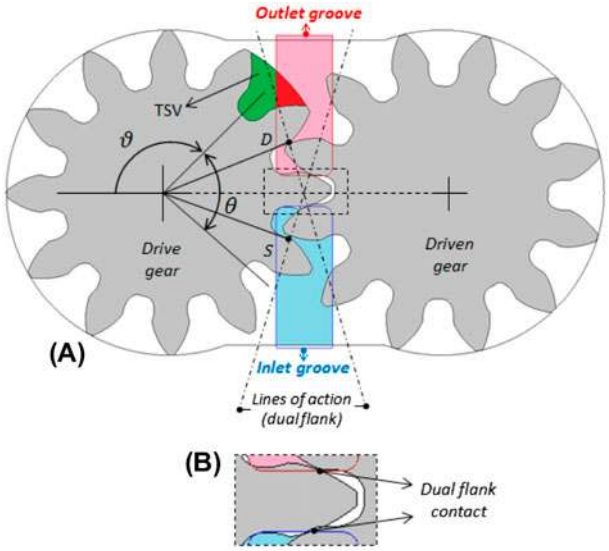

Figure 3. (A) Generic TSV at angular position ϑ and the angular interval θ in which the meshing process takes place, Groove positions in the slider to achieve max displacement. (B) TSV with dual flank contact configuration.

where a TSV at a generic angular position ϑ is represented, and in Figure 4, a typical trend of the TSV over a shaft revolution is also depicted.

The displacing action occurs in the angular interval θ, which defines the meshing region. Between points D and S of the line of action, the TSV is trapped between points of contact, therefore the displacing action is realized by means of the inlet/outlet grooves (the trace of these grooves is indicated in Figure 3(A). In standard EGMs, the commutation between inlet and outlet groove is realized when the volume is minimum, so that the maximum volumetric capacity of the pump is utilized. Ideally, this commutation occurs without crossport areas, so that for each TSV the volume indicated in the Figure 4

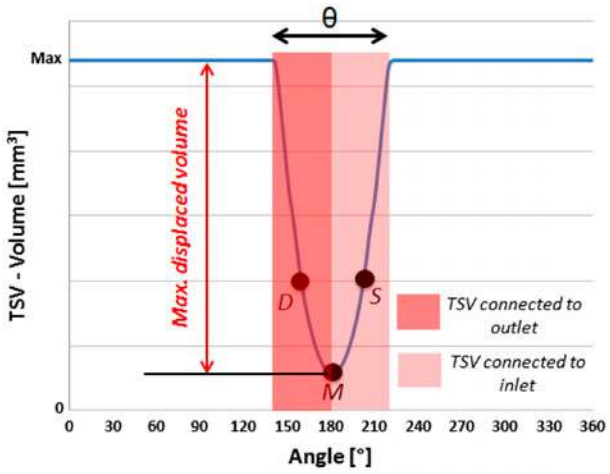

Figure 4. TSV as a function of shaft angle showing the angular interval in which the TSV is connected to the outlet and the inlet for achieving maximum displacement. The switch of the TSV connection from the outlet to inlet occurs when the TSV is at its minimum (M).

can be displaced; however, the optimal performance in terms of noise reduction, limitation of internal pressure peaks and cavitation is realized with a small crossport (Borghi *et al*. 2006, Eaton *et al*. 2006).

For the case considered in this work, for which a dual-flank contact condition is realized by the gears (Figure 3(B)), considerations about the TSV on the drive or driven gear are similar as shown in Figure 4. However, for a single-flank contact unit, due to the presence of a backlash between the gears, each TSV of the drive gear is connected to a correspondent TSV of the driven gear. Therefore, considerations concerning the displaced volume of the unit should refer to the union of this TSV pair, and not to the isolated TSVs as described in this section.

While in standard EGMs the mentioned inlet/outlet grooves are machined in the lateral bushings or in the unit housing (for low pressure, non-pressure compensated designs), in the proposed design the slider contains these grooves. The one degree of freedom for the slider position permits to vary the position of these grooves, hence affecting the angular position at which the commutation between the connections of each TSV with the inlet/outlet ports is realized. The effect of different positions of the slider can be described with Figure 4 and Figure 5. As shown in Figure 4 the TSV is connected to the inlet and outlet for equal intervals of time, therefore, the maximum flow is displaced by the unit.

However, a reduced displacement is achieved when the slider is positioned closer to the inlet port (as shown in Figure 5(A)). This is because each TSV remains connected to the outlet port for a first portion of the filling process, (after it reaches the minimum volume point at 180°), wherein a part of the fluid already delivered to the outlet is taken back into the TSV which acts as the fluid "virtual dead volume." Due to this "dead volume,"

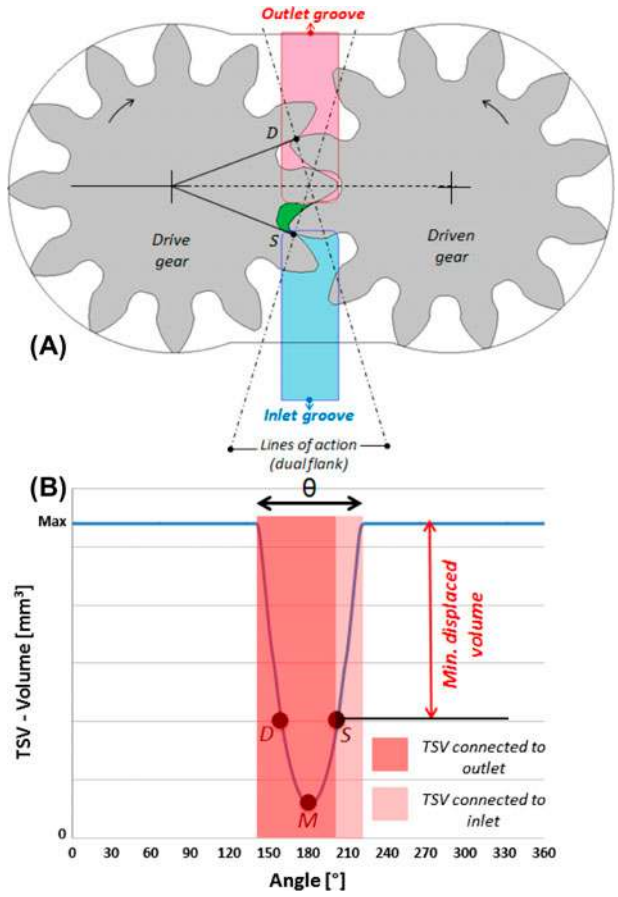

Figure 5. (A) Position of the grooves in the slider to achieve min. displacement. The switch of the TSV connection from the outlet to inlet occurs when the TSV is at point S. (B) TSV as a function of shaft angle showing the angular interval in which the TSV is connected to the outlet (larger red box) and the inlet (small pink box) for achieving reduced displacement.

each TSV is capable of displacing a reduced volume of fluid. Graphically, the principle can be represented by a larger (as compared to Figure 4) portion connected to the delivery (in red, in Figure 4 and Figure 5(B)) and a smaller portion in which the TSV is connected to the inlet (in blue, in the same figures). The additional "dead volume" is equal to the difference between the volumes of points S and M, therefore the effective fluid displaced to the outlet is equal to the difference between the maximum volume and volume at point S.

It is important to observe how the variation of the achieved displacement as a result of change in slider position can occur for all slider positions that realize the described switching between the points D and S, in which each TSV is trapped between points of contact of the teeth. By moving the slider outside the limits D-S a direct bypass connection between the outlet and the inlet would be realized, hence significantly reducing the volumetric efficiency of the VD-EGM. With symmetric gears, the points D and S lie very closely to point M and hence they do not offer a large variation in the displacement, therefore novel asymmetric gear profiles are used to maximize the reduction in displacement (as described in §3 and §4)

To realize delivery flow variation, the slider can move either towards the inlet port (as shown in Figure 5) or towards the outlet port. However, being the conditions of the fluid at the inlet port often close to saturation (for the case of a pump), it is preferable to consider the motion towards the inlet port, so that cavitation effects due to fluid aeration are limited. The opposite consideration apply for the case of a motor.

Figure 6 qualitatively represents the forces due to the pressure acting on the gears for both max. and min. displacements, for the case of a pump. The resultant of the high pressure acting on a larger area of the gears, lead to lower forces as depicted by the arrows of different lengths in Figure 6. But what is more important is that the reduced displacement configuration of Figure 6(B), by extending the high pressure region in the meshing zone, introduces a torque contribution towards shaft rotation, thus lowering the torque adsorption of the pump. It has to be noticed how both figures assume perfect sealing of the TSVs in the low pressure/inlet side, which is a realistic condition as described in Vacca and Guidetti (2011). However, the torque reduction principle still holds also with different assumption for the pressure distribution at the peripheral of the gears, such as the one described in (Ivantysyn and Ivantysynova 2001).

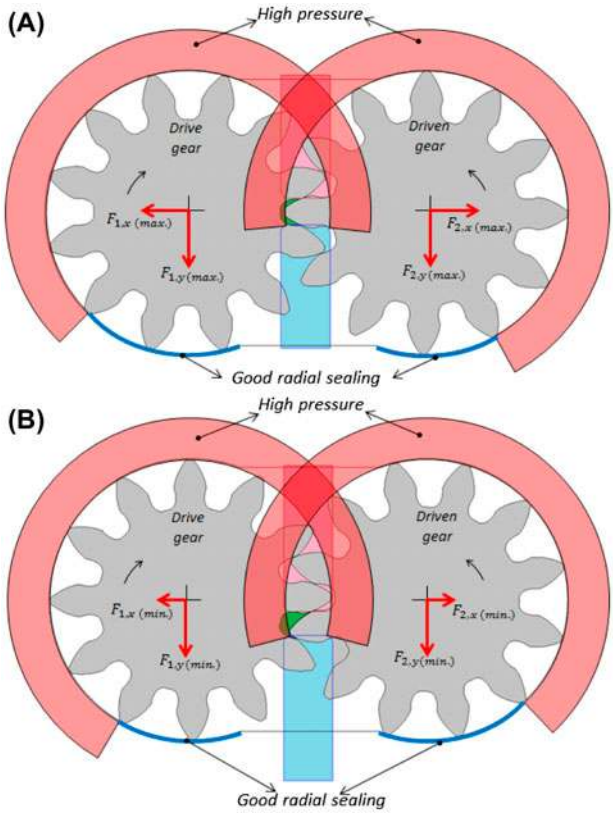

Figure 6. (A) Qualitative representation of the forces acting on the gears at max displacement. (B) Qualitative representation of the forces acting on the gears at min displacement.

With the description given above, one can notice how the proposed VD- EGM realizes a similar variable timing principle of digital pumps/motors investigated by several authors for radial and axial piston units (Ehasan *et al*. 1996, Nieling *et al*. 2005, Merrill *et al*. 2013). However, while mentioned solutions are capable of reaching a full displacement variation range (0%–100%), they require electronically controlled fast on/off valves to realize the variable connections of each displacement chamber with the inlet and outlet port. In the considered design, the slider remains at a fixed position to realize certain unit displacement, and it has to be moved only to realize a different displacement value. Therefore, this implementation does not require fast components, and the flow variation strategy does not necessarily require electronic control (pure hydraulic pressure or flow compensators can be realized with the slider).

A variable timing concept similar to the one described in this paper for VD-EGM was proposed by Manco *et al.* (2004) for the case of gerotor pumps. In this design a variable angular position of the port plate was introduced to vary the effective flow displaced by the displacement chambers of the unit. Also in this solution a variation in delivery flow was obtained at the expense of lower torque. However, the introduction of a rotating port plate appears to significantly increase the cost of the unit.

3. Definition of the gear profile

Gears with asymmetric teeth profile, unconventional for EGMs, were investigated in this work with the particular aim of maximizing the range of displacement variation achievable for the VD-EGM with the concept described in §2. In the past, only few published studies focused on the design of gears different from symmetric involute profile. Kumar *et al.* (2008), Kapelevich (2000) focused on analyzing the benefits of using asymmetric profiles for power transmission applications (not in EGMs). However, Nagamura *et al.* (2004), Devendran and Vacca (2013a) implemented asymmetric gears in EGMs particularly focusing on fluid-borne-noise reduction. A similar design approach as in (Devendran and Vacca 2013b) will be used in a different optimization framework for determining the optimal design of the gears for the proposed VD-EGM as described in §6.

In this work, the design of the gears is assumed to be comprised of involute and trochoid profiles above and below the base circle respectively. In order to accomplish the goal of designing asymmetric teeth, two different pressure angles are considered respectively for the drive and opposite coast tooth flanks as shown in Figure 7. In order to ensure that the asymmetrical teeth gear profile is physically manufacturable using conventional manufacturing processes like hobbing, shaping, rack-cutting etc., an asymmetrical cutter profile is assumed at first. The tooth profile is then derived on the basis of the shape of the asymmetric cutter as shown in Figure 7. Based on

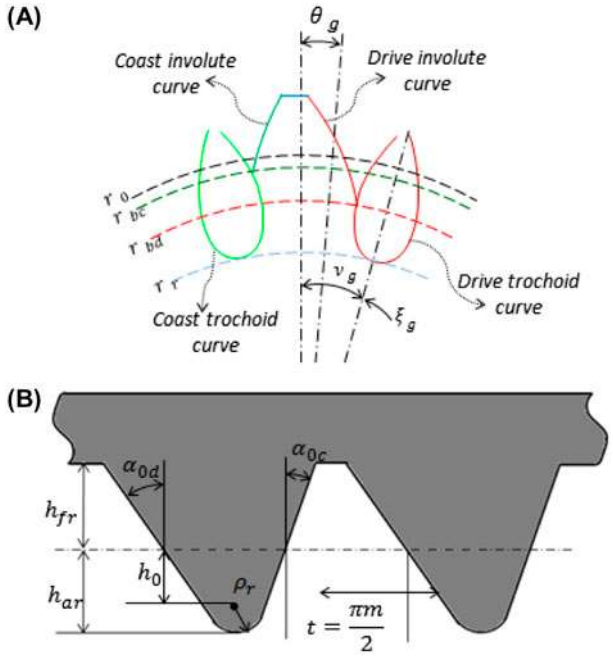

Figure 7. (A) Drive and coast sides of a gear tooth depicting the involute and trochoid profiles. (B) Asymmetric tool profile taken as reference for generating gears.

the design variables, the parameters which govern the shape of the asymmetric cutter are obtained using Eqs. (1) – (4), (Nagamura *et al.* 2004).

$$h_{ar} = 1.25 \cdot m \tag{1}$$

$$h_{fr} = 1 \cdot m \tag{2}$$

$$\rho_r = \frac{(\pi \cdot m/2) - (\tan\alpha_{od} + \tan\alpha_{oc}) \cdot h_{ar}}{(1/\cos\alpha_{0d}) + (1/\cos\alpha_{oc}) - (\tan\alpha_{od} + \tan\alpha_{oc})} \tag{3}$$

$$h_0 = h_{ar} - \rho_r \tag{4}$$

The involute profiles for both the drive and coast side of the teeth can be obtained using the Eqs. (5) – (7) (Nagamura *et al.* 2004). These equations are represented in a generic form for any involute side of the teeth, changing the values of r_b and ϑ_g for the drive or coast yields respectively the corresponding involute profiles as shown in Figure 7.

$$x = (\sin\theta_g - \theta_g \cdot \cos\theta_g) \cdot r_b \cdot \cos\vartheta_g - (\cos\theta_g + \theta_g \cdot \sin\theta_g) \cdot r_b \cdot \sin\vartheta_g \tag{5}$$

$$y = (\sin\theta_g - \theta_g \cdot \cos\theta_g) \cdot r_b \cdot \sin\vartheta_g + (\cos\theta_g + \theta_g \cdot \sin\theta_g) \cdot r_b \cdot \cos\vartheta_g \tag{6}$$

where,

$$\vartheta_g = \mathrm{inv}\alpha_0 + \frac{\pi}{2 \cdot z} \tag{7}$$

Similar to the construction of the involute profiles, the trochoid profiles of the teeth are obtained using the

generic Eqs. (8) – (10), as shown in Figure 7 (Nagamura *et al.* 2004).

$$x = (r_0 - h_0) \cdot \sin(\xi_g + v_g) - r_0 \cdot \xi_g \cdot \cos(\xi_g + v_g) - \left[\frac{r_0 \cdot \xi_g + h_0}{\sqrt{h_0^2 + r_0^2 \cdot \xi_g^2}}\right] \cdot \rho_r \cdot \sin(\xi_g + v_g) \quad (8)$$

$$y = (r_0 - h_0) \cdot \cos(\xi_g + v_g) + r_0 \cdot \xi_g \cdot \sin(\xi_g + v_g) + \left[\frac{r_0 \xi_g - h_0}{\sqrt{h_0^2 + r_0^2 \xi_g^2}}\right] \cdot \rho_r \cdot \sin(\xi_g + v_g) \quad (9)$$

where,

$$v_g = \frac{\pi}{2 \cdot z} + \frac{h_0 \cdot tan\alpha_0}{r_0} + \frac{\rho_r + b_n}{r_0 \cdot \cos\alpha_0} \quad (10)$$

The value of b_n controls the backlash in the gear pair generated; therefore setting its value to zero yields gears with zero backlash or dual flank contact.

4. Definition of the inlet and outlet groove profiles

In the VD-EGM, the grooves machined in the lateral bushings (or in the housing, for not pressure compensated designs) perform the important timing function of connecting TSVs with the inlet or outlet environment when the TSV is trapped between points of contact. Therefore, they contribute in determining the amount of fluid displaced per revolution by every TSV. With an optimal crossport (simultaneous connection of the TSV with the inlet and outlet port), the grooves can also ensure minimal internal pressure overshoots and localized cavitation effects during the transition of TSV from/to the low pressure and high pressure regions. For the asymmetric gear profile considered in this research, a particular "two-winged" structure of the grooves was considered as shown in Figure 8(A).

The different parameters which control the shape of the grooves are depicted in Figure 8. The main intent for using such a two winged architecture with four angular controls (α's) is to understand the influence of the pressure angles (drive and coast side) of the gear profiles on the performance of the machine. Particular emphasis is placed on the feasibility of machining the grooves using the conventional milling process for prototyping. As can be seen from Figure 8, the radius "R" of the milling tool is taken into consideration, so the optimal design out of the optimization process can be directly prototyped without any additional consideration based on manufacturability.

5. Hydraulic gear machines simulator

In this work, the simulation of the performance for any given geometrical configuration of the VD-EGM is based on the HYGESim (HYdraulic GEar machines Simulator)

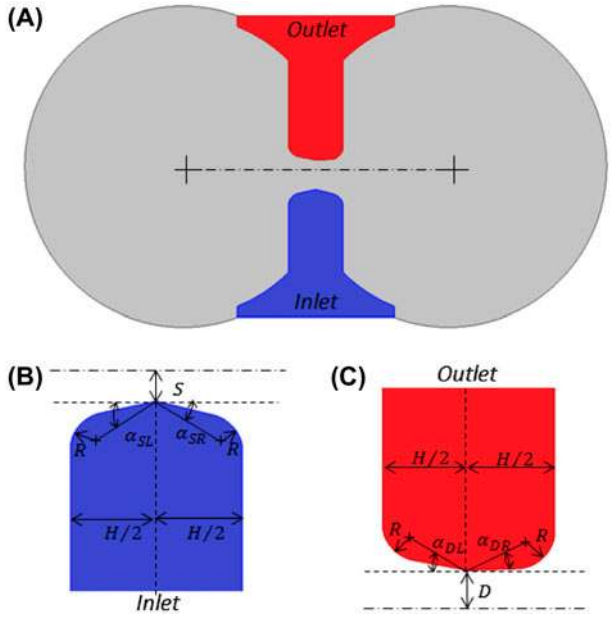

Figure 8. (A) Lateral bushings with a representative inlet and outlet grooves. (B) Detail of the inlet groove. (C) Detail of the outlet groove.

tool developed by the author's team. Several past publications covered the development of this simulation tool, therefore in the following only the main features of the tool are summarized.

The geometric model of HYGESim evaluates all the geometrical features necessary to perform the fluid dynamic simulation of the unit. Originally conceived on standard involute profiles (Vacca and Guidetti 2011), the geometrical model was recently extended to permit simulation of asymmetric gear profiles (Devendran and Vacca 2013a), with an additional module used to directly generate the design of both gears and grooves without recourse of CAD drawings.

A lumped parameter approach is at the basis of the fluid dynamic model and the model for the evaluation of micro-motions of the gears rotation axis. This model is implemented within built in routines in AMESim® and permits to evaluate all the features of the flow through the EGM, including inlet and outlet flow and pressure, flow through the TSV, instantaneous meshing pressure. An accurate evaluation of radial leakages, at the tip of each tooth, is performed considering the actual position of the gears, resulting by a force balance that include contact forces and pressure forces. Recently, additional functionalities for the evaluation of fluid properties accounting for transient fluid aeration were introduced in HYGESim (Zhou *et al.* 2014). Without going to the details of the implementation of the lumped parameter approach of the main fluid dynamic model, which can be found in (Vacca and Guidetti 2011), the basic equations used to determine the pressure in the TSV volumes and the flow through the connections between adjacent volumes are reported with Eqs. (11) and (12)

$$\frac{dp_i}{dt} = \left.\frac{1}{V_i}\frac{dp}{d\rho}\right|_{p=p_i} \cdot \left[\sum \dot{m}_{in,i} - \sum \dot{m}_{out,i} - \rho|_{\rho=\rho_i}\left(\frac{dV_i}{dt} - \frac{dV_{var,i}}{dt}\right)\right] \quad (11)$$

$$\dot{m}_{i,j} = \frac{(p_i - p_j)}{|(p_i - p_j)|} \cdot \rho|_{P=\overline{P_{i,j}}} \cdot \alpha \cdot \Omega_{i,j} \cdot \sqrt{\frac{2 \cdot (p_i - p_j)}{\rho|_{P=\overline{P_{i,j}}}}} \quad (12)$$

A separate Fluid Structure Interaction model is developed using C++ O-Foam libraries for the simulation of the lateral lubricating gaps in EGMs (Dhar and Vacca 2013). Due to computational time required to run this latter module of HYGESim, not suitable to perform numerical optimization as in this study, for the study of the VD-EGM prototype of this work, the lateral lubricating gap was assumed to be as a constant gap.

Finally, HYGESim can be used within the commercial AMESim® tool, permitting the simulation of the EGM in a generic hydraulic system by combining the EGM model with the model of the inlet/outlet circuit connected to the unit.

6. Optimization process

In this research, the optimal design of the asymmetric gears along with their grooves is determined using a multi-level-multi-objective genetic algorithm-based optimization process. A schematic of the complete optimization workflow is shown in Figure 9. As depicted in Figure 9, *Level 1* deals entirely with the design of asymmetric gears and *Level 2* deals with the optimization of the grooves in the lateral bushings. Due to the inherent inter-relationship existing between the design of the gears and the grooves, a design process considering an optimization within an optimization is of extreme importance and necessity. Once the gears are designed in *Level 1*, the contact points between the gear teeth are tracked throughout an entire revolution of the gears. Particularly, the location of the points D and S (defining the angular locations at which the fluid in the TSV is trapped between the contact points between the gears) is identified, followed by the geometric evaluation of the progress of the TSV. Finally, the amount of displacement reduction that can be achieved in with the design of the gears is evaluated.

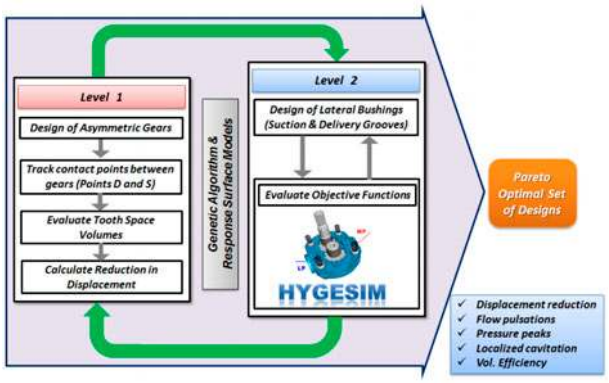

Figure 9. Schematic of the multi-level multi-objective optimization process.

Following the design of the gears, the optimization algorithm moves automatically into *Level 2*: entirely dedicated to the determination of the optimal design of the grooves for the particular gear designed in *Level 1*. In *Level 2*, the simulation tool HYGESim is used as a "virtual test rig" to evaluate the performance of the machine in a particular hydraulic test circuit required by the user. Post processing the results of HYGESim, yields the values of the different objective functions (OFs). These OFs are related to the performance of the unit in terms of capability of varying the delivery flow, maintaining high volumetric efficiency with smooth meshing process. Level 2, automatically performs enough number of iterations until an optimal design of the grooves is determined. The OFs corresponding to the particular combination of the gears and the grooves is conveyed to Level 1 for enabling comparison with other gear designs also operating with their optimal groove counterparts. This procedure thus enables the determination of the optimal design of the machine as a "whole."

Due to the different nature of the OFs (described in details in §6.1), which are not directly related to each other, conventional optimization algorithms such as linear, quadratic programming, sequential quadratic programming and other gradient-based algorithms cannot be easily applied. For this reason a genetic algorithm capable of handling the vastly varying and complex design space was used. The algorithm takes advantage of response surface models – such as surrogate modeling and kriging – to perform a virtual optimization of the response surfaces to identify the designs in a more efficient and quicker process. This process thus provides a number of designs which satisfy all the objective functions at a Pareto optimum, from which the user has the freedom of choosing the best design which fits their specific requirements (Poloni *et al*. 2000).

The described optimization procedure derives its motivation from (Devendran and Vacca 2012–13a,b) wherein a similar method was used to optimize EGMs for low noise emissions, however; mentioned works did not consider the evaluation of the reduction in displacement along with the other performance features.

The following sub-sections details the formulation of the objective functions as well as of the constraints used in this procedure.

6.1. *Objective functions*

Five different OFs are used in the multi-objective optimization procedure of Figure 9. These are specifically given by: 1. possible reduction in displacement, 2. delivery flow pulsations, 3. internal pressure overshoots, 4. localized cavitation effects and 5. volumetric efficiency.

Maximize reduction in displacement (OF_1)

The maximum reduction in displacement can be calculated at the level 1 of the optimization procedure, by investigating the location of the points D and S (which define the angular locations at which the fluid in the TSV is trapped between the contact points between the gears) in the curve that characterize the volume of each TSV, as shown in Figure 10.

Due the asymmetric nature of the gears, the location of the points "D" and "S" (which represents the angular location when the TSV is trapped) are not symmetric about the point "M" (angular location which the trapped TSV is at a minimum) unlike gears with symmetric involute teeth (as shown in Figure 10).

It can be seen however that the angular range remains at the same point ($\theta_D 2 - \theta_S 2 = \theta_D 1 - \theta_S 1$) though the actual position at which these points occur differs as seen Figure 10. Since dual flank configuration is imposed on all the gears, and in order to expand further the angular range of the trapped volume, both the drive TSV and driven TSV behave as two independent displacing chambers which are not connected to each other. Therefore, to maximize the full potential in achieving the reduction in displacement, the switch of the connection of the drive TSV from the delivery to suction should occur at point S1, and at point S2 for the TSV on gear 2 since both TSVs operate as separate displacement chambers due to the introduction of dual flank configuration.

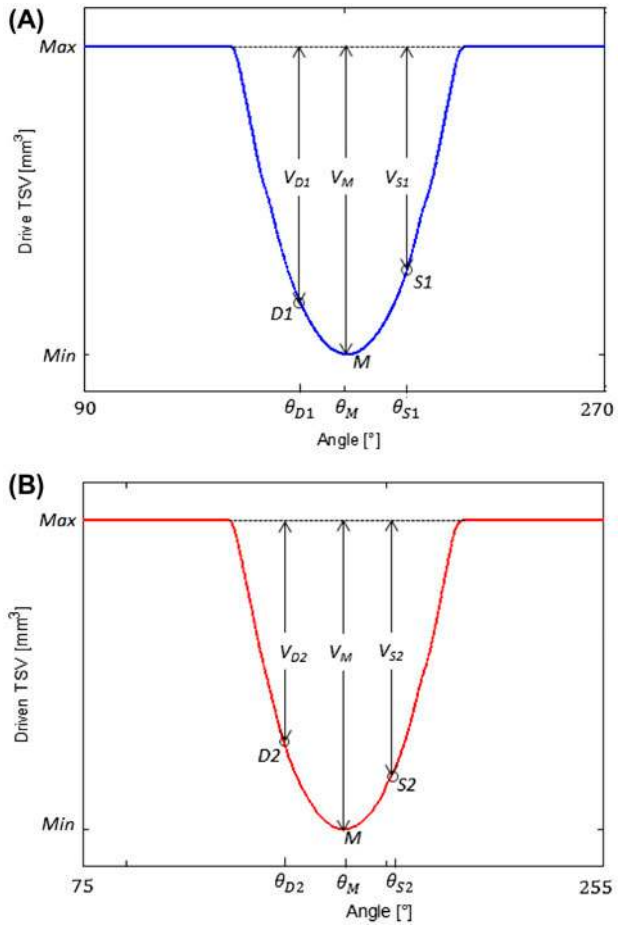

Figure 10. (A) Drive TSV for asymmetric gears with dual flank contact configuration. (B) Slave/driven gear TSV for asymmetric gears with dual flank contact configuration.

The resultant minimum displacement achievable can be expressed as an average of the ones provided by the drive and the slave/driven TSVs independently. The minimum displacement achievable can be calculated using Eq. (13)

$$\beta = \frac{\beta_{drive} + \beta_{driven}}{2} = \frac{V_{S2} + V_{S1}}{2 \cdot V_M} \tag{13}$$

Therefore, the objective function for maximizing the reduction in displacement can be expressed as Eq. (14).

$$Maximize : OF_1 = 1 - \beta \tag{14}$$

Minimize delivery flow ripple (OF_2)

Port flow fluctuation is one of the main contributions to the fluid borne noise (Fiebig 2007, Opperwall and Vacca 2013). An accurate estimation of the port flow ripple can be done using the energy associated to each peak in the frequency spectra of the signal. Therefore, an estimate of OF_2 can be expressed as the sum of squares of the amplitude corresponding to the fundamental harmonics obtained after a Fast Fourier Transform (FFT) of the flow ripple. Eq. (15) (Vacca *et al.* 2007) represents the expression for OF_2,

$$Minimize : OF_2 = \sum_{k=1}^{N} \pi_k, \quad where\, \pi_k = \sum_{f_k - f}^{f_k + f} L(f)^2 \tag{15}$$

Where, N is the total number of fundamental harmonics of interest. π_k is the total energy of k^{th} fundamental frequency about a frequency resolution, Δ_f and $L(f)$ is the FFT of the flow ripple signal.

Minimize internal pressure peaks (OF_3)

Pressure peaks associated with the fast reduction of the TSV during the meshing process need to be reduced to reduce noise and increase machine reliability. HYGESim is capable of accurately predict local peaks (Zhou et al, 2014). OF_3 is expressed as a non-dimensional value given by, Eq. (16).

$$Minimize : OF_3 = \frac{P_{TSV,max} - P_{D,avg}}{P_{D,avg}} \tag{16}$$

Minimize localized cavitation (OF_4)

After displacing fluid to the outlet, the TSV is filled with fluid from the inlet during the second part of the meshing

process. The rapid increase of the volume can lead the pressure in the TSVs to fall below the saturation pressure of the fluid. The minimum pressure level depends on the connections of the TSV with the inlet port; therefore localized cavitation occurring during the meshing process can be limited by using a proper design of the inlet grooves. OF_4 is expressed (as Eq. (17)) as the area of the TSV pressure curve which falls below the saturation pressure of the fluid (Devendran and Vacca 2013a,b)

$$Minimize : OF_4 = \int P_{TSV} d\theta, \quad \forall P_{TSV} < P_{sat} \tag{17}$$

Maximize volumetric efficiency (OF_5)

The performance of the EGM in terms of volumetric efficiency needs to be maximized. The expression for OF_5 is given by Eq. (18).

$$Maximize : OF_5 = \eta_v = \frac{Q_{avg}}{n \cdot V_d} \tag{18}$$

Where, Q_{avg} is the mean flow provided by the machine at its delivery while operating at a speed of n rpm and V_d is the displacement of the machine. In this study the conditions at maximum displacement are considered for the evaluation of OF_5.

6.2. Inputs and constraints

The design variables governing the shape of the gears and the grooves are represented in Table 1 and Table 2 respectively. Without proper constraints, the optimization would be capable of choosing any combination of the different design parameters. With that, many designs would be unfeasible considering the working of the machine as well as its manufacturability. Therefore, several constraints were formulated to ensure the validity of all designs taken into consideration by the procedure.

Contact ratio: In order to ensure the smooth transmission of forces between the gears, there should be at least one pair of teeth which is always in contact with each other (for load sharing) during the working of the machine (Litvin and Fuentes 2004). Therefore the contact ratio for both the sides of the gears, (namely the drive and the coast) should always be greater than one (a thumb rule is to use this value as 1.1) as shown in Eq. (19).

Table 1. Design variables for gears.

		Range		
Variable	***Unit***	***min***	***max***	***Step***
m	mm	1.0	3.6	m
z	–	9.0	24	z
α_{0d}	°	5.0	30.0	α_{0d}
α_{0c}	°	5.0	30.0	α_{0c}

Table 2. Design variables for inlet and outlet grooves.

		Range		
Variable	***Unit***	***min***	***max***	***Step***
D	mm	0.0	3.6	D
S	mm	0.0	3.6	S
R	mm	0.5	2.0	R
α_{DL}	°	−45.0	12	α_{DL}
α_{DR}	°	−45.0	12	α_{DR}
α_{SL}	°	−45.0	12	α_{SL}
α_{SR}	°	−45.0	12	α_{SR}

$$\varepsilon = \frac{2 \cdot \sqrt{r_a^2 - r_b^2} - m \cdot z \cdot \sin\alpha}{\pi \cdot m \cdot \cos\alpha} > 1.1 \tag{19}$$

Interference: The process when the corresponding drive or the coast sides of both the gears intersect with each other is known as interference. With interference, the gear teeth are weakened due to the removal of the material near the root of the gears (Litvin and Fuentes 2004). Based on the limiting case of interference when the tip circle of one gear is below the base circle of the other gear, the generic expression for this constraint for both the drive and coast sides of the teeth are derived, Eq. (20)

$$r_a^2 < r_b^2 + 4 \cdot r_0^2 \cdot \sin^2\alpha \tag{20}$$

Pointed teeth: This constraint restricts the optimization algorithm from generating gears which have very sharp tooth tips, hence, preventing the wear and tear of the casing due to the sharp gears. The constraint can be expressed as (Litvin and Fuentes 2004):

$$2 \cdot r_a \cdot \left(\frac{\pi}{2 \cdot z} + inv\ \alpha - inv\ \alpha_a\right) > 0.30 \tag{21}$$

Facewidth (b) of the gears is calculated based on the displacement (V_d) of the machine which is assumed at the beginning of the optimization process. Since the gears considered are asymmetric, the facewidth (b) of the gears can be expressed as Eq. (22),

$$b = V_d / \left(2 \cdot \pi \left[r_a^2 - \frac{r_o^2}{\cos\alpha_{0d} + \cos\alpha_{0c}} \cdot \left(2\cos\alpha_{0c} + \frac{\pi^2 \cdot \cos^3\alpha_{0c}}{6 \cdot z^2}\right)\right]\right) \tag{22}$$

Additional constraints for the gears were enforced on the addendum radius and the face width of the gears so that the gears generated will fit inside a commercial pump for experimental testing and validation (as described in §8).

Bending stress: When the loads are too large, bending failure may occur. Bending failure in gears is predicted by comparing the calculated bending stress to the maximum allowable stress values (Shigley and Mischke 1996). The bending stress number for a gear can be calculated as,

$$S_t = \frac{W_t \cdot K_a}{K_v} \cdot \frac{1.0}{b \cdot m} \cdot \frac{K_s \cdot K_m}{J}. \quad (23)$$

This number is related to the allowable bending stress number, S_{at} and therefore the constraint can be represented as,

$$S_t \leq \frac{S_{at} \cdot K_L}{K_T \cdot K_R}, \quad (24)$$

Hence, ensuring the non-failure of the generated gears due to bending.

Pitting resistance: Pitting of the gear flanks are caused by alternating normal pressure on the contact surfaces of the teeth due to the mechanical vibrations. It is found to occur most frequently at the pitch circle-where relative sliding of the teeth is zero, thereby causing high surface failure due to the removal of the material from the tooth surface due to the high contact stresses between the mating gears (Shigley and Mischke 1996).

The expression for evaluating pitting resistance or surface durability of a gear tooth can be written as,

$$S_c = C_p \sqrt{\frac{W_t \cdot C_a}{C_v} \cdot \frac{C_s}{d \cdot b} \cdot \frac{C_m C_f}{I}}, \quad (25)$$

The contact stress number, S_c is related to the allowable contact stress number, S_{sc} and therefore the constraint can be represented as,

$$S_c \leq S_{ac} \cdot \frac{C_L \cdot C_H}{C_T \cdot C_R}, \quad (26)$$

Hence, ensuring the non-failure of the generated gears due to pitting.

*Groove*s: The constraints for the grooves specifically ensure that both the grooves do not intersect with each other as expressed by Eq. (27) (valid for the left (L) and the right (R) sides of the grooves), so as to prevent direct bypass of the fluid from the high pressure region to the inlet through the TSV.

$$\frac{\pi m}{2}(\cos\alpha_{0d} + \cos\alpha_{0c}) - \left(\frac{r_a - r_r}{2}\right)\begin{pmatrix}\tan\alpha_D \\ +\tan\alpha_S\end{pmatrix} + \mathrm{S} + \mathrm{D} + \mathrm{R} > 0.60 \quad (27)$$

In order to reduce the number of design variables for the *level 2* of optimization and hence improving the speed of the optimization, the horizontal length of the grooves is maintained to be constant as shown by Eq. (28)

$$H = r_a - r_r \quad (28)$$

7. *Simulation results*

In this section, the optimal design obtained at the end of the optimization process is presented along with simulation results concerning the delivery flow, tooth space pressure, force, torque etc. Around 900 gear designs were simulated with 60 grooves design in the automated optimization process. The optimal design was identified at the end of over 500 hours of computation (on a Dell® Precision T1600 workstation, with Intel® Xeon® processor). Several design configurations of gears and grooves were simulated in the autonomous design optimization process. In order to ensure the possibility of testing the optimal design, the optimization was constrained in such a way that the gears generated will be able to fit inside the casing of commercial gear machine. Therefore, the facewidth, inter-axis distance (and hence the pitch diameter), and outer radius of the gears were constrained to that of the commercial gear pump with specification mentioned in Table 3.

Optimal Design

The optimal design of the gears which provided maximum reduction in displacement, while maintaining all the other performance parameters at an optimum is shown in the Table 4. It is observed that the optimal design chosen is capable of offering a remarkable range of variation of displacement for 100% (max.) to 68% (min.). Particularly, the design of the gears was partly constrained (outer radius and face-width) by the requirement of fitting them in an existing commercial pump body to limit the costs of the experimental activity; hence the results were limited achieving 68% min. displacement. However, it should be noted that a more aggressive design with displacement variation up to 60% was also obtained with teeth of low thicknesses and unconventionally low pressure angle values, but these designs were not considered for the first proof-of-concept tests.

The optimal design for both the gears and the grooves in the lateral bushing are shown in Figure 11.

The delivery flow predictions for max and min displacement at two different operating conditions are shown in Figure 12. It can be seen that the delivery flow at min displacement is 68% of that provided at 100% displacement, hence, proving the concept for variable delivery EGMs. It can also be noticed that in all these operating conditions, the flow oscillations at min.

Table 3. Specification of the reference pump.

Displacement	11.20 cc/rev
Number of teeth per gear	12
Facewidth	17 mm
Max. operating pressure	280 bar
Max. operating speed	3500 rpm

Table 4. Design parameters for the optimal design.

Displacement	*11.90 cc/rev*
Number of teeth per gear	*16*
Drive pressure angle	*9.50°*
Coast pressure angle	*5.00°*
Minimum Displacement	***68 % (8.09 cc/rev)***

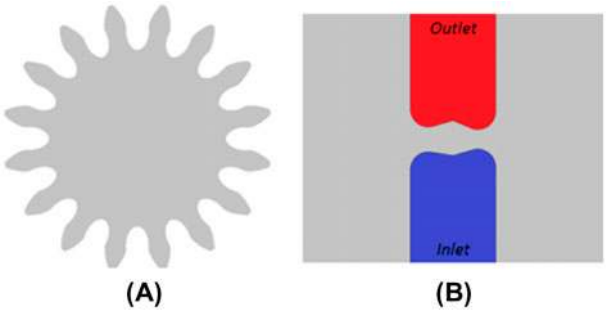

Figure 11. (A) Optimal design of the gear (B) Optimal design of the grooves.

displacement, (β = 68%) is higher than that at max. displacement. An explanation for this is the fact that the optimization process took into consideration the groove design only at max displacement, and the same groove shape is moved with the help of the slider towards the suction/inlet side. Therefore, the performance was not simultaneously optimized for both max and min displacement.

Tooth Space Pressures

The drive tooth space pressures (driven tooth space pressures follow similar trends) for two different operating conditions are shown in Figure 13.

It can be seen that for almost all the operating conditions considered, the TSV pressure peak is very close to being negligible which proves that the design of the grooves is at an optimum. Also at 2000 rpm the TSV pressure peak is about 20 bar above the delivery pressure; this is an acceptable value, is similar to those predicted in commercially available pumps (Zhou *et al.* 2014). As evidently visible from these figures, the tooth space pressure for min displacement (β = 68%) extends for a larger time period as depicted by the red curves, because the TSVs are connected to the delivery/outlet groove for a larger time period to bring about a reduction in displacement

Forces acting on the gears

The horizontal component of the total force acting on the drive gear (due to pressure and contact forces) is depicted in Figure 14. It can be seen that at all the operating conditions, the horizontal component of force has a negative value reflecting the direction of action of forces (direction pointing from the center of the gears towards the casing). It can also be observed that at min displacement the magnitude of force is less compared to that at max displacement, since the gears are exposed to a larger time period (as can be seen from Figure 13) in the high pressure zone, at min displacement. A similar trend of reduction in horizontal forces is also observed for the driven gear.

Total Torque required at the shaft

The input torque predictions for both max/min displacement at two different operating conditions are shown in Figure 15. It can be seen that the required torque at min

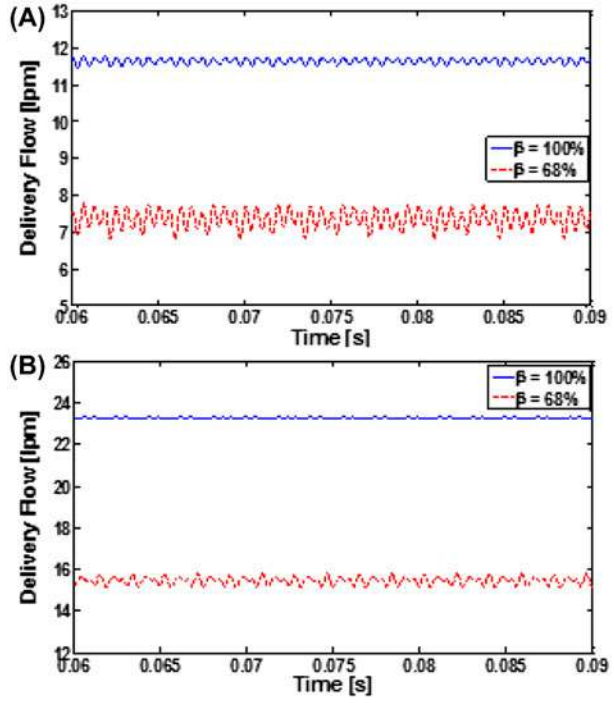

Figure 12. (A) Delivery flow at 100% and 68% disp. for 1000 rpm, 100 bar. (B) Delivery flow at 100% and 68% disp. for 2000 rpm, 200 bar.

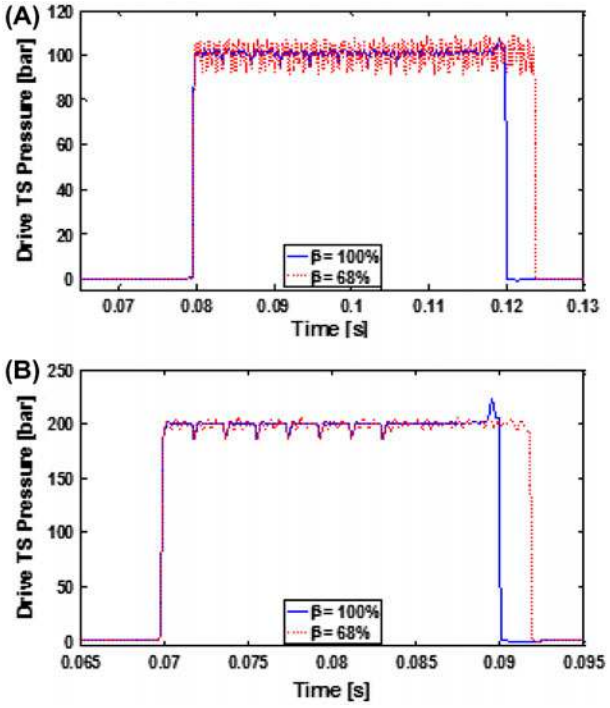

Figure 13. (A) Tooth space pressure at 100% and 68% disp. for 1000 rpm, 100 bar. (B) Tooth space pressure at 100% and 68% disp. for 2000 rpm, 200 bar.

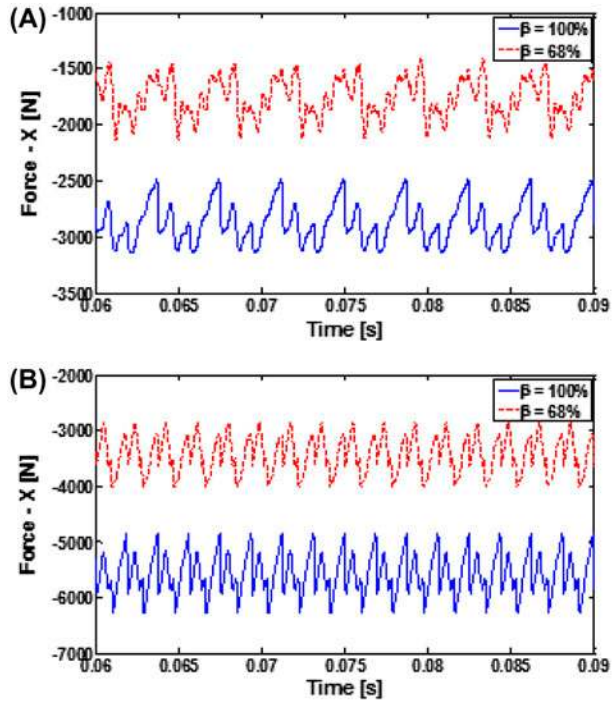

Figure 14. (A) Horizontal component of force acting on the drive gear at 100% and 68% disp. for 1000 rpm, 100 bar. (B) Horizontal component of force acting on the drive gear at 100% and 68% disp. for 2000 rpm, 200 bar.

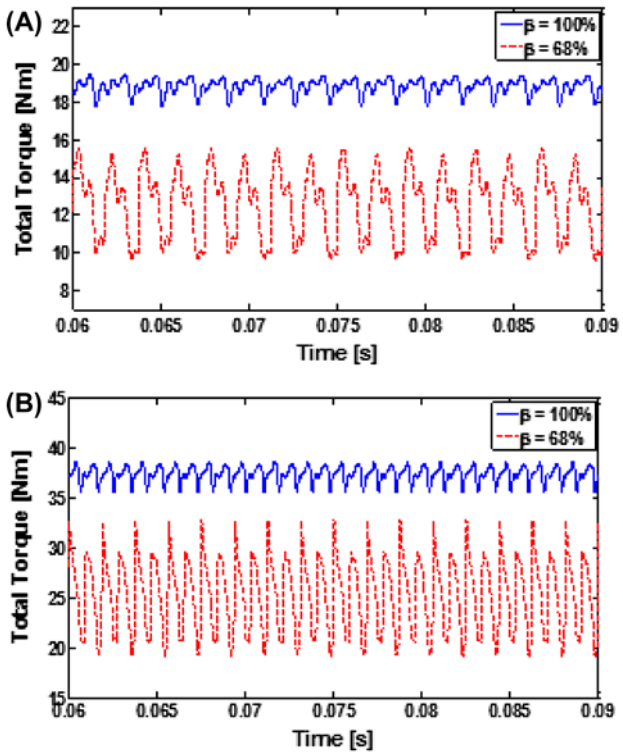

Figure 15. (A) Total torque required at 100% and 68% disp. for 1000 rpm, 100 bar. (B) Total torque required at 100% and 68% disp. for 2000 rpm, 200 bar.

displacement is about 68% of that provided at 100% displacement, due to the lower total force acting on the gear as explained previously. The lower input shaft torque required reflects on the lower energy consumption at min. displacement, thus supporting the viability of a VD-EGM.

It can be seen from these figures, that the oscillations of the shaft torque are higher at min displacement as compared to that at max displacement. Also in this case, a possible explanation is given to the fact that the optimal design of the machine was identified considering only on minimizing the flow/torque pulsations at max displacement. However, the amplitudes of the oscillations are in line and similar with that of commercial pumps, hence these oscillations are not expected to be adversely affecting the performance of the machine in a negative manner.

8. Proof of Concept Tests

The encouraging performance potentials obtained in simulations for a wide range of operating conditions, provided motivation for designing a proof of concept test, whose primary goal is to prove the principle behind the proposed VD-EGM.

8.1. Prototype design

The optimal design of the gears with asymmetric teeth (as previously shown in Figure 11) was manufactured using a wire electric discharge machining process (Wire EDM) for prototyping process. Additional finishing operations and heat treatment processes, which would guarantee longer live and reduced operating noise were not performed on the gears since the sole purpose of the tests was to prove the working concept of the proposed VD-EGM. For this reason, the tests were carried out at a limited pressure (p_{max} – 100 bar). The final prototyped gears (drive and driven) assembled inside the casing is depicted in Figure 16.

In order to validate the VD-EGM principle, it is not necessary to implement a moving slider in the lateral bushings. Instead, two different lateral bushings with different groove designs corresponding to max and min displacement (as shown in Figure 16 (B) and (C)) can be used to determine the performance at the two respective desired levels of displacement. It should be noted that, the grooves for min. displacement were designed at the limit of achieving the min. displacement considering only the volumetric performance of the machine. However, these grooves were not optimized for minimizing flow pulsations, since the purpose of the tests was to understand the maximum potential of operation of a VD-EGM and to validate the results in terms of displacement reduction alone.

8.2. Experimental Test Setup

Experimental measurements were performed at Maha Fluid Power Research Center of Purdue University. The

Figure 16. (A) Prototype optimal gears assembled within the commercial casing. (B) Lateral bushings with grooves for max. (100%) displacement. (C) Lateral bushings with grooves for min. (68%) displacement.

objective of the experiments was to measure the steady state performance parameters of the units working as pump for two different delivery flow levels. The hydraulic circuit used for the test is in accordance with ISO 4409 standard for pump characterization. In particular, an electric motor was used to drive the pump; the driveline was also equipped with an optical speed measurement system and a torquemeter. The outlet pressure for the EGM was set using a variable orifice at the desired value, and the suction and the delivery lines were equipped with thermocouples, pressure sensor and flowmeter. A system of coolers and heaters integrated in the test-rig permits a closed loop control of fluid temperature at EGM inlet.

All testing conditions were performed with an inlet temperature of 50˚C within a range of ± 1˚C using a ISO VG46 oil (Density: 846.9 kg/m^3, Bulk Modulus: 13703 bar at 50˚C and atmospheric pressure).

The pump casing used for the test was the same of a commercial pump used as reference. It has to be noted how this casing was previously broken-in by the pump manufacturer (the initial wear of casing induced by this process significantly affect the volumetric efficiency of the unit (Vacca and Guidetti 2011)). About the test procedure, steady state measurements were first performed on the commercial gear pump, after which the pump was dismantled and the commercial gears and the lateral bushings were removed and substituted with the prototype gears and the lateral bushings for max displacement and measurements were conducted. Following this step, the pump was disassembled again and only (prototype gears remain the same) the lateral bushings for min displacement were replaced with those for max displacement, and measurements were performed.

8.3. *Experimental Results and Validation*

In this section, the results of the proof of concept tests particularly concerning delivery flow rate, input shaft torque are presented.

The results of the experiments are compared with those of the simulations provided by HYGESim for a wide range of operating conditions.

It can be seen from Figure 17 that the flow rate proportionally (68%) reduces at min displacement as compared to those at full or max. displacement. A good agreement between simulated data and measurements can be observed from the figure. However, at both displacements there is a small offset between the two curves which can be explained by the low tolerance of the process used to realize the gears. Apparently, the gears do not permit to strictly maintain the dual flank contact conditions for all teeth into mesh (a more expensive gear cutting process would be required to guarantee this condition); as a consequence, an imperfection in achieving zero backlash between the gears is introduced, and a certain amount of bypass leakage is introduced from the high pressure to the low pressure side through the TSVs hence causing an lower volumetric performance in the experiments.

Figure 18 represents the input shaft torque validation. It can be seen that the input shaft reduces proportionally at min displacement. Approximately 32% reduction in torque is obtained at all the operating conditions tested for min displacement. The simulations under-predict the input shaft torque because the shear losses in the lateral gaps as well as the effect of friction due to the sliding of

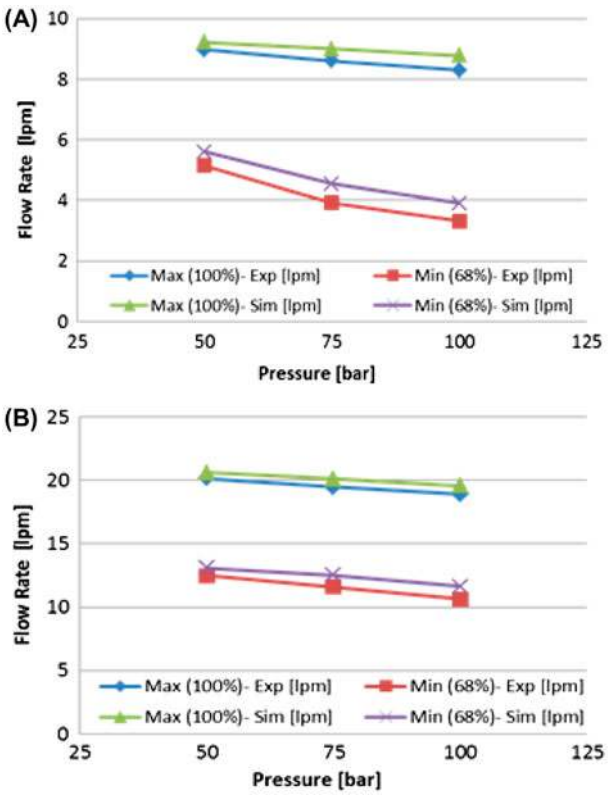

Figure 17. (A) Validation for flow rate at max and min disp. for 1000 rpm. (B) Validation for flow rate at max and min disp. for 2000 rpm.

the gear teeth with each other have not been considered in the simulations.

The validations for volumetric efficiency are reported in Figure 19. Firstly, the blue curve (diamond dots) represents the performance of the reference commercial EGM (of the same displacement). It can be noticed that the volumetric performance at max displacement, as shown by the orange curve (square dots) matches very closely to that of the reference design (shown by the blue curve with diamond dots). The minor discrepancies evident from the figure can be attributed to the fact that a dedicated break-in process for the asymmetric gears was not realized. As a consequence, bigger internal leakages at the tip of each tooth were expected for the prototype gears.

It should also be noted that the volumetric efficiency for all the pressures at max. and min. displacement is higher for 2000 rpm (Figure 19(B)) as compared to 1000 rpm (Figure 19(A)), this is because the maximum speed at which the casing was broken in was 2000 rpm and hence the gears are capable of achieving better radial sealing thereby leading to better volumetric performance at 2000 rpm.

As expected, it can be seen from Figure 19that the volumetric efficiency at min displacement is lower than the volumetric efficiency at max. displacement. This is due to the fact that the internal leakages (at the tip of the teeth and in the lateral side of both gears) are most

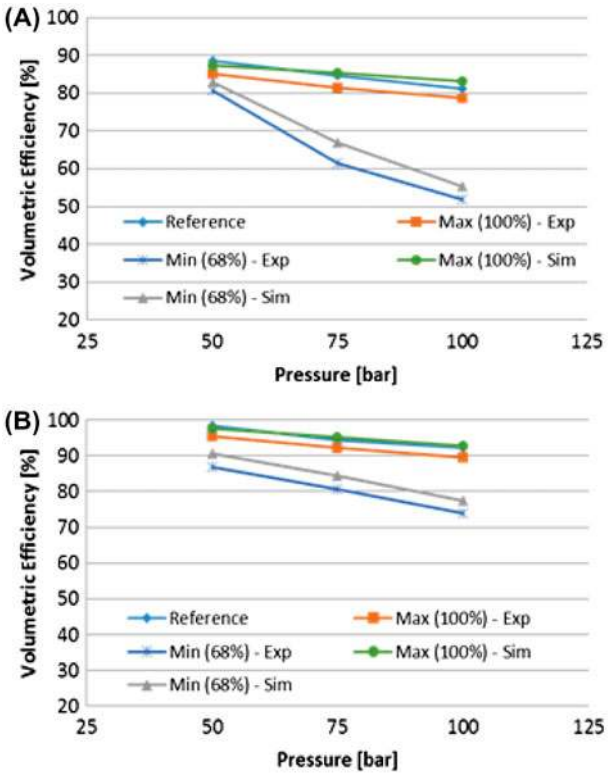

Figure 19. (A) Validation for vol. efficiency at max and min disp. for 1000 rpm. (B) Validation for vol. efficiency at max and min disp. for 2000 rpm.

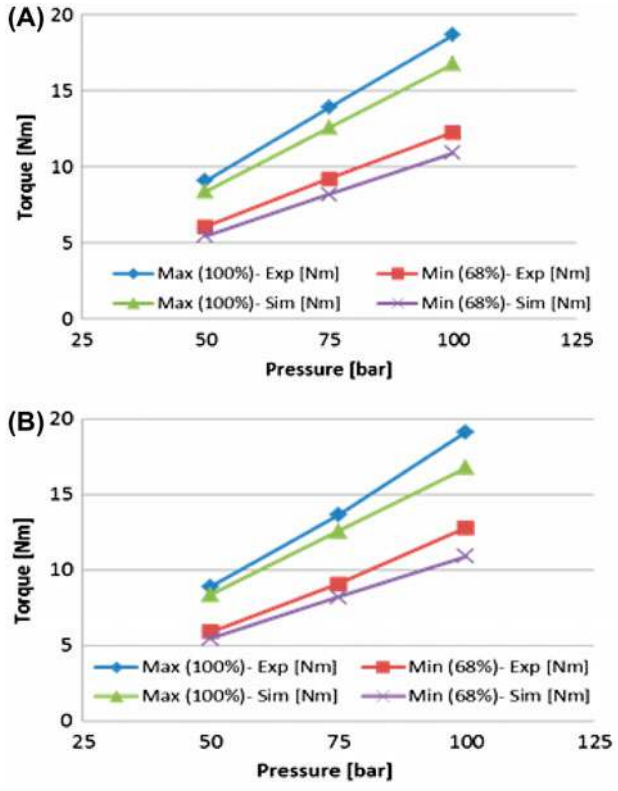

Figure 18. (A) Validation for input torque at max and min. disp. for 1000 rpm. (B) Validation for input torque at max and min disp. for 2000 rpm.

prominently dependent on the pressure and hence have a larger influence for the efficiency at lower displacement. The trends of simulated volumetric efficiency at min. displacement matches pretty closely to that of the measured values, thereby purporting the capabilities of HYGESim to predict the performance of the VD-EGM at varying levels of displacement.

9. Conclusion

The current study presents an innovative approach for a working concept for variable delivery flow external gear machine (VD-EGM). The main idea behind the VD-EGM is based on the realization of a variable timing for the connections of the TSVs with the inlet and outlet, which can be realized through the introduction of a movable element (slider) at gears lateral side.

In order to maximize the range of variation of displaced flow, a non-conventional design for the gears based on asymmetric teeth profiles was considered.

A multi-level and multi-objective optimization workflow was created to determine the optimal design of the gears and of the grooves machined on the slider simultaneously. This optimal design permits the maximization of the allowable range of flow variation, but also permits to maximize volumetric efficiency, limit the pressure pulsation and guarantee a smooth meshing process without internal pressure peaks or localized cavitation.

The resulting design offered a remarkable 32% reduction in displaced flow (from 100% flow to 68% flow) while maintaining all the other performance features at an optimum. It should be noted that this results was in part limited by the requirement of fitting the resulting gears in an existing commercial pump body to limit the costs of the experimental activity.

Simulation results performed on a pump showed that the delivery flow rate as well as the input shaft torque reduced proportionally based on the reduction in displacement predicted.

An experimental campaign was also performed to prove the numerical predictions and confirm the validity of the proposed principle for VD-EGMs. Measurements were in line with the expectations, and confirmed the concept of reducing flow as well as shaft torque with the proposed concept.

Although the proposed concept cannot achieve a full (0–100%) flow regulation as other variable displacement units, the proposal of a cost effective solution for partially variable displacement unit (such as the proposed design) will permit to substitute current fixed displacement units with significant energy advantages. As a matter of fact, in many fluid power applications the hydrostatic units are sized for the peak demand of flow, that have operating cycles in which the unit idles for significant time intervals. This additional flow-on-demand capability will permit to reduce the energy losses associated with phases of non-full utilization of the hydrostatic unit.

The future work for the topic includes the optimization of the groove profiles considering the performance of the machine at both max and min displacement. Also, a working prototype of VD-EGM inclusive of a movable slider will be realized and tested.

Acknowledgement

This research was supported by the Center for Compact and Efficient Fluid Power (CCEFP), a National Science Foundation (NSF) Engineering Research Center (Project 1F.1) funded under cooperative agreement number EEC-0540834.

Nomenclature

Symbol	Description	Units
C_f	Surface condition factor	[-]
C_p	Elastic coefficient of the material	[MPa$^{1/2}$]
D	With respect to gears: the point at which the trapped tooth space volume begins to exist With respect to grooves: vertical distance of the delivery groove from the line joining the inter-axis of the two gears	[mm]
H	Horizontal dimension of the delivery and suction grooves	[mm]
J,I	Geometry factor for bending strength and pitting resistance	[-]
K_H, C_H	Hardness ratio for bending strength and pitting resistance	[-]
K_L, C_L	Life factor for bending strength and pitting resistance	[-]
K_T, C_T	Temperature factor	[-]
K_R, C_R	Reliability factor	[-]
K_a, C_a	Application factor for bending stress and pitting resistance	[-]
K_m, C_m	Load distribution factor for bending strength and pitting resistance	[-]
K_s, C_s	Size factor for bending strength and pitting resistance	[-]
K_v, C_v	Dynamic factor for bending strength and pitting resistance	[-]
P	Pressure in the TSV	[bar]
$P_{D,avg}$	Average pressure at the delivery	[bar]
P_{sat}	Saturation pressure of the operating fluid	[bar]
$P_{TSV,max}$	Pressure in the tooth space volume	[bar]
Q_{avg}	Average delivery flow rate	[lpm]
S	With respect to gears: the point at which the trapped tooth space volume seizes to exist With respect to grooves: Vertical distance of the suction groove from the line joining the inter-axis of the two gears	[mm]
S_t	Bending stress number	[MPa]
W_t	Maximum transmitted load to the gears	[N]
Z	Number of teeth	[-]
k	Index for the fundamental frequency of the FFT	[-]
m	Normal module	[mm]
$\dot{m}$	Mass flow rate	[kg/s]
r_a	Addendum radius	[mm]
r_o	Pitch radius	[mm]
r_b	Base circle radius	[mm]
r_r	Root circle radius	[mm]
r_{bd}	Drive side base circle radius	[mm]
r_{bc}	Coast side base circle radius	[mm]
t	Tooth thickness of the gear cutter	[mm]
α_{DL}	Angular position of the left wing of the delivery groove	[°]
α_{DR}	Angular position of the right wing of the delivery groove	[°]
α_{SL}	Angular position of the left wing of the suction groove	[°]
α_{SR}	Angular position of the right wing of the suction groove	[°]
α_0	Pressure angle	[°]
α_a	Pressure angle at the addendum circle	[°]
α_{0d}	Drive pressure angle	[°]
α_{0c}	Coast pressure angle	[°]
β	Percentage displacement of VD-EGM	[%]
η_v	Volumetric efficiency	[%]
ρ	Density of the operating fluid	[kg/m^3]
ρ_r	Root fillet radius of the rack cutter	[mm]
θ_g, ϑ_g	Involute co-ordinate parameters	[°]
v_g, ξ_g	Trochoid co-ordinate parameters	[°]
Ω	Orifice area of the connections between the two TSVs	[mm^2]

Abbreviations

EGM	External Gear Machine
OF	Objective function
TSV	Tooth Space Volume
VD	Variable delivery
Avg	Average
Deliv	Delivery

Disp	Displacement
Ref	Reference value
Max	Maximum value
Min	Minimum value

Notes on contributors

Ram Sudarsan Devendran received his Masters' degree in Mechanical Engineering from Purdue University in 2012. Currently he is a PhD candidate whose research interests include the development of a novel design of variable displacement type external gear machines. Also, his research focusses on optimization of the designs of the external gear machines focusing on unconventional gear profiles, based on a multitude of performance features.

Andrea Vacca received his Masters' degree in Mechanical Engineering from the University of Parma (Italy) in 1999 and his Doctorate in Energy Systems from the University of Florence (Italy) in 2005. He is currently an Associate Professor for the School of Mechanical engineering as well the Agricultural & Biological Department. His current research includes a broad range of analysis, modeling and testing of fluid power systems and hydraulic components. Particular goals of his research are the improvement of energy efficiency and controllability of fluid power systems and the reduction of noise emissions of fluid power components. To accomplish the goals of his research, Prof. Vacca's research team has developed original numerical techniques to simulate fluid power systems and components, especially gear machines and hydraulic control valves.

References

Borghi M., *et al*., 2006, *The influence of cavitation and aeration on gear pump and motors meshing volume pressures*, IMECE2006, ASME Int. Mechanical Engineering Congress and Exposition, 5–10 November, Chicago, IL, USA.

Bowden, C., 1989, *Variable discharge gear pump with energy recovery*, Patent Application Publication, US4824331.

Bowden, C., 1990, *Variable discharge gear pump with energy recovery*, Patent Application Publication, US4902202.

Bussi, E., 1992, *Variable delivery gear pump*, European Patent Application, EP0478514.

Clarke, J.M., 2002, *Hydraulic transformer using a pair of variable displacement gear pumps*, Patent Application Publication, US2002104313.

Devendran, R.S. and Vacca, A., 2013a, *Design potentials of external gear machines with asymmetric tooth profile*, Proceedings of the ASME/Bath Symposium on Fluid Power & Motion Control, 6–9 October, Sarasota, FL, USA.

Devendran, R.S. and Vacca, A., 2013b. Optimal design of gear pumps for exhaust gas aftertreatment applications. *Simulation Modelling Practice and Theory*, 38, 1–19.

Devendran, R.S. and Vacca, A., 2012, *Optimal design of gears and lateral bushes of external gear machines*, Proceedings of the Bath/ASME Symposium on Fluid Power and Motion Control, 10–12 September, Bath, UK.

Dhar, S. and Vacca, A., 2013. A fluid structure interaction-EHD model of the lubricating gaps in external gear machines: formulation and validation. *Tribology International*, 62, 78–90.

Eaton, M., Keogh, P.S., Edge, K.A., 2006, The Modelling, Prediction, and Experimental Evaluation of Gear Pump Meshing Pressure with Particular Reference to Aero-Engine Fuel Pumps. *Proceedings of the Institution of Mechanical Engineers, Part I: Journal of Systems and Control Engineering*, 220–365.

Ehasan, M, Rampen, W.H., and Salter, S.H., 1996. *Computer Simulation of the Performance of Digital Displacement Pumps-Motors*. ASME International Mechanical Engineering Congress and Exposition, 19–24, Atlanta, GA, USA.

Fiebig, W. 2007. Location of Noise Sources in Fluid Power Machines. *International Journal of Occupational Safety and Ergonomics*, 13 (4), 441–450.

Hoji, T., Nagao, S., Shinozaki, K. 2008 *Gear Pump*, Patent Application Publication, US2008044308.

Ivantysynova, M. 1998. *Pump Controlled Actuator – a Realistic Alternative for Heavy Duty Manipulators and Robots*. International Scientific Forum in Fluid Power Control of Machinery and Manipulators, Cracow, Fluid Power Net Publication, 2000 (5), 101–123.

Ivantysyn, J. and Ivantysynova, M. 2001. *Hydrostatic Pumps and Motors, Principles, Designs, Performance, Modelling, Analysis, Control and Testing*. New Delhi. Academia Books International, ISBN -81-85522-16-2.

Kapelevich, A., 2000. Geometry and Design of Involute Spur Gears with Asymmetric Teeth. *Mechanism and Machine Theory*, 35, 117–130.

Kumar, V.S., Muni. D.V., and Muthuveerappan. G., 2008. Optimization of Asymmetric Spur Gear Drives to Improve the Bending Load Capacity. *Mechanism and Machine Theory*, 43, 829–838.

Litvin, F.L. and Fuentes, A., 2004. *Gear Geometry and Applied Theory*. 2nd ed. Cambridge University Press.

Mahrenholz, J. and Lumkes, J.J., 2009. Model Development and Experimental Analysis of a Virtually Variable Displacement Pump System. *International Journal of Fluid Power*, 10 (3), 17–27.

Manco, S., Nervegna, N., and Rundo, M., 2004, *Displacement vs Flow Control in IC Engines Lubricating Pumps*. Proceedings of the 2004 SAE World Congress, (2004-01-1602), Detroit, MI, USA.

Merrill, K., Breidi, F.Y., and Lumkes, J., 2013. *Simulation Based Design Optimization of Digital Pumps/Motors*, ASME/Bath Symposium on Fluid Power and Motion Control, 6-9 October, Sarasota, FL, USA.

Murrenhoff, H., Sgro, S., Vukovic, M., 2014, *An Overview of Energy Saving Architectures for Mobile Applications*, Proceedings of 9th International Fluid Power Conference, 24–26 March , Aachen, Germany.

Nagamura, K., Ikejo, K. and Tutulan, F.G., 2004. Design and Performance of Gear Pumps with a Non-Involute Tooth Profile. *Proceedings of the Institution of Mechanical Engineers, Part B: Journal of Engineering Manufacture*, 218, 699–711.

Nieling, M., Fronczak F.J., Beachley N.H., 2005. *Design of a Virtually Variable Displacement Pump/Motor*. Proceedings of the 50th National Conference on Fluid Power, Las Vegas, 2005.

Opperwall, T. and Vacca, A., 2013. A combined FEM/BEM model and experimental investigation into the effects of fluid-borne noise sources on the air-borne noise generated by hydraulic pumps and motors, *Proceedings of the Institution of Mechanical Engineers, Part C: Journal of Mechanical Engineering Science*, 1–15.

Poloni, C., *et al*., 2000. Hybridization of a Multi-Objective Genetic Algorithm, a Neural Network and a Classical

Optimizer for a Complex Design Problem in Fluid Dynamics. *Computer Methods in Applied Mechanics and Engineering*, 186, 403–420.

Rannow, M.B. Li, P.Y., 2009. *Soft Switching Approach to Reducing Transition Losses in an ON/OFF Hydraulic Valve*. Proceedings of the ASME 2009 Dynamic Systems and Control Conference, 12–14 October, Hollywood, California, USA.

Reiners, W. and Wiggermann, W., 1960, *Variable Delivery Gear Pumps*. The Patent Office London, GB968998.

Shigley, J.E. and Mischke, C.R., 1996, *Standard Handbook of Machine Design*. 2nd ed. Mc Graw Hills, New York, NY, USA.

Tomlinson, S.P. and Burrows, C.P., 1992. Achieving a Variable Flow Supply by Controlled Unloading of a Fixed- Displacement Pump. *ASME Journal of Dynamic Systems Measurement and Control*, 114 (1), 166–171.

Vacca, A. and Guidetti, M. 2011. Modelling and experimental validation of external spur gear machines for fluid power applications. *Simulation and Modeling Practice and Theory*, 19, 2007–2031.

Vacca A., Franzoni G., and Casoli, P., 2007, *On the Analysis of Experimental Data for External Gear Machines and their Comparison with Simulation Results*, ASME International Mechanical Engineering Congress and Exposition, 11–15 November, 2007, Seattle, WA.

Winmill, L.F., 2001. *Adjustable-Displacement Gear Pump*. Patent Application Publication, US2001024618.

Yang, D. Zhong, D., 1987, *Radial-Movable Variable Displacement Gear Pump (Motor)*. CN85109203.

Zhou, J., Vacca, A., and Casoli, P., 2014. A Novel Approach for Predicting the Operation of External Gear Pumps under Cavitating Conditions. *Simulation Modeling Practice and Theory*, 45, 35–49.